RSC Advances

PAPER

View Article Online
View Journal | View Issue

Cite this: *RSC Adv.*, 2022, **12**, 4322

Synthesis of UV/blue light-emitting aluminum hydroxide with oxygen vacancy and their application to electrically driven light-emitting diodes†

Heejae Lee, *[a] Ahyoung Hong,[b] Jeonghun Kwak [b] and Seonghoon Lee[a]

Aluminum hydroxide nanoparticles, one of the essential luminescent materials for display technology, bio-imaging, and sensors due to their non-toxicity, affordable pricing, and rare-earth-free phosphors, are synthesized *via* a simple method at a reaction time of 10 min at a low temperature of 200 °C. By controlling the precursor's ratio of aluminum acetylacetonate to oleic acid, UV or blue light-emitting aluminum hydroxides with oxygen defects and carbonyl radicals can be synthesized. As a result, aluminum hydroxide ($Al(OH)_{3-x}$) nanoparticles overwhelmingly emit UVA light (390 nm) because of the oxygen defects in nanoparticles, and carbon-related radicals on the nanoparticles are responsible for the blue-light emission at 465 nm. Electrically driven light-emitting devices are applied using luminescent aluminum hydroxide as an emissive layer, that consists of a cost-efficient inverted bottom-emission structure as [ITO (cathode)/ZnO/emissive layers/2,2′-bis(4-(carbazol-9-yl)phenyl)-biphenyl (BCBP)/MoO_3/Al (anode)]. The device with aluminum hydroxide as an emissive layer shows a maximum luminance of 215.48 cd m^{-2} and external quantum efficiency (EQE) of 0.12%. The new method for synthesizing UV–blue emitting aluminum hydroxides and their application to LEDs will contribute to developing the field of non-toxic optoelectronic material or UV–blue emitting devices.

Received 28th October 2021
Accepted 26th January 2022

DOI: 10.1039/d1ra07942e

rsc.li/rsc-advances

Introduction

Luminescent inorganic materials, such as oxide-based inorganic phosphors, quantum dots, carbon dots, rare-earth phosphors, and metal hydroxides, have been researched for display, sensor technology, solar energy conversions, LEDs, bio-imaging, and more for their luminescent properties and chemical stability.[1–12] Among different luminescent materials, aluminum-related materials with bandgaps above 4.5 eV, such as aluminum oxide (Al_2O_3), aluminum hydroxide ($Al(OH)_3$), and boehmite (AlOOH), have attracted attention due to their low cost, high stability, and non-toxicity. They have different origins of light emission from luminescent nanoparticles such as quantum dots which controlled the band gap between 1.2–3.5 eV depending on their size or shape (*i.e.*, quantum confinement effect).[8,10] Since defects and color centers in aluminum-related materials can substantially affect the materials' electrical, optical, and thermal properties, those materials have also been studied for applications of optoelectronic devices.[2,13–16] Especially, various polymorphs of an aluminum hydroxide such as gibbsite, bayerite, nordstrandite, and doyleite have been produced and applied to micro-organism and phosphate absorbents for waste treatment, antacid drugs, and flame retardant materials.[2,14] Recent studies have shown that aluminum hydroxide exhibits strong photoluminescence properties with high quantum yields owing to the presence of oxygen vacancies and carbon doping.[12,14,16,18] It is important to investigate those optical phenomena in order to widen its applications to optical sensors, LEDs, waste treatment, medical science, *etc.*[3,4,6,9,13–20] As demonstrated in previous works, aluminum hydroxide nanomaterials emit UVA light (383–400 nm) due to their oxygen vacancy (F^+ center, *i.e.*, one electron trapped at an anion vacancy) and blue light (450–470 nm) caused by carbon related radical impurities on the surface from the decomposition of metal–organic precursor or organic compound such as aluminum diacetate hydroxide, aluminum triacetate, benzoyl alcohol, oxalic acid, *etc.*[13–21] Additionally, the faintly green light emission (500–550 nm) is presented owing to the hydroxyl group and carbon compounds (such as Al–OH, CO_2, 1,2,3,4-tetrahydrocarbazole, *etc.*) on the surface of aluminum hydroxide particles.[12,14,16,18] Recently, aluminum hydroxide materials that emit UV and blue light with photoluminescence quantum yields (PLQYs) 38–65% with ~100 nm of the full width at half maximum (FWHM) have been made in

[a]*School of Chemistry, Seoul National University, Seoul 08826, Republic of Korea. E-mail: heejaelee@snu.ac.kr*

[b]*School of Electrical and Computer Engineering, Inter-University Semiconductor Research Center, Seoul National University, Seoul 08826, Republic of Korea*

† Electronic supplementary information (ESI) available. See DOI: 10.1039/d1ra07942e

various forms such as nanoplates, rods, fibers, wires, and particles by using CVD, pulsed laser ablation (PLA), and a sol–gel method at harsh conditions of 320 °C or higher with a long synthesis duration of 20–72 hours.[4,12,14,16–18] Due to their optical properties, emissive aluminum hydroxide have been applied to solar photovoltaics by combining with polymers to form a polymeric composite luminescent film, and to UV-pumped white LEDs (which use UV-LED chips emitted at 370–407 nm of wavelength) with a color rendering index (CRI) value of 94.[12,16–18] So, a straightforward synthetic method and application to UV–blue light-emitting diodes are highly needed. In this study, amorphous aluminum hydroxide nanoparticles ($Al(OH)_{3-x}$) with oxygen defect and carbonyl radical on the surface were rapidly obtained by the simple synthetic method at a low temperature of 200 °C for 10 minutes using a base catalyst. By adjusting the ratio of aluminum acetylacetonate ($Al(acac)_3$) and oleic acid (OA) as precursors, we obtained two types of amorphous $Al(OH)_{3-x}$ with different photoluminescence (PL) intensity of emitting wavelengths. One was dominantly emitting at 390 nm with a maximum PLQY of 71% and 35 nm of a FWHM, which was named Sample-A, and the other which named Sample-B was emitting at 395 nm and 465 nm with a narrow FWHM (35–43 nm) and a PLQY of 30% and 67%, respectively. The photoluminescence (PL) peak at 390 nm and the photoluminescence excitation (PLE) peak at 370 nm were provided that the $Al(OH)_{3-x}$ we made was amorphous phase with oxygen defect (F^+ center). And we applied electron paramagnetic resonance (EPR) spectroscopy, a sensitive technique for detecting paramagnetic defects of materials, to address the possible presence of carbon-related radical species produced by the decomposition of metal–organic precursors in our samples which might be the source of emission peak at 465 nm. Additionally, luminescent $Al(OH)_{3-x}$ nanoparticles we made were presented for the electrically driven active LEDs structure, which quantum dot-based LEDs research has been well known.[8,10,22–24] The $Al(OH)_{3-x}$ based LEDs were efficiently fabricated by the solution processing method. The architecture of the active LEDs with $Al(OH)_{3-x}$ emissive layers (EML) was ITO (cathode)/ZnO nanoparticle films (40 nm)/$Al(OH)_{3-x}$ active layers (~2 monolayers)/2,2′-bis(4-(carbazol-9-yl)phenyl)-biphenyl (BCBP, 50 nm)/MoO_3 (10 nm)/Al (100 nm). As a result, the device with a Sample-A emitting layer had an electronic performance with a maximum brightness of 215.48 cd m^{-2} at 10.4 V, turn-on voltage of 5.6 V, and external quantum efficiency (EQE) of 0.12%. It is expected to be applied to UV-LED to replace UV-lamp, which contains mercury or metal halide toxic gas. The other device with the emitting layer of Sample-B shown a turn-on voltage of 8.0 V, a brightness of 133.49 cd m^{-2} at 13.4 V, and the maximum EQE was 0.09%. Device performances we obtained are comparable with making the UV-visible emitting active LEDs based on graphene QD, CdZnS QDs, and carbon dots as a light-emitting layer with EQE of 0.02–0.24% at 7–17 V.[11,23,25–28] The optical property, chemical stability, non-toxicity, and EL characteristics of $Al(OH)_{3-x}$ we presented will be used as a potential luminescent phosphor candidate for application in next-generation UV–blue lighting and display technology.

Results and discussion

Synthesis of amorphous aluminum hydroxide nanoparticles

The luminescent amorphous aluminum hydroxide ($Al(OH)_{3-x}$) was quickly synthesized at 200 °C for 10 minutes using aluminum acetylacetonate ($Al(acac)_3$), oleic acid (OA), and lithium bis(trimethylsilyl)-amide (Li-HMDS) solution acted as the base catalyst. To synthesize two types of amorphous $Al(OH)_{3-x}$ samples with different luminescence properties named Sample-A and B, $Al(acac)_3$ and OA were dissolved in 10 mL of 1-octadecene at a ratio of 1 : 3.5 and 1 : 2.4, respectively. After degassing at 120 °C to remove H_2O or O_2, amorphous $Al(OH)_{3-x}$ nanoparticles were quickly created by injecting Li-HMDS solution to the transparent solution at 200 °C. The optical properties of the synthesized nanoparticles are depicted in Fig. 1. In the case of Sample-A, the highest photoluminescence intensity was found at 390 nm wavelength (λ_{max}^{PL}) at excitation of 375 nm, as shown in Fig. 1(a). They have 71% of a relative photoluminescence quantum yield (PLQY) compared to 9,10-diphenyl anthracene organic dye (λ_{max}^{PL} 406 nm, QY 90%) at room temperature. For the excitation wavelength of 430 nm, the PLQY reaches up to 48% at λ_{max}^{PL} of 450 nm (compared to coumarin 515, λ_{max}^{PL} 478 nm, QY 80%). When excitation was performed at 500 nm, it was found to have photoluminescence λ_{max}^{PL} at 537 nm with 37% of PLQY (compared to rhodamine 590, λ_{max}^{PL} 550 nm, QY 95%). As seen in Fig. 1(b), Sample-B has similar emission wavelengths as Sample-A, but the photoluminescence intensity of that wavelength is different. The Sample-B emits light at 395 nm, 465 nm, and 527 nm with PLQYs of 30%, 67%, and 53%, respectively. Images for each graph of Fig. 1(a) and (b) show that $Al(OH)_{3-x}$ solutions dissolved in hexane emit under natural sun-light (left side) and 365 nm-UV lamp (right side) at room temperature. There are different pathways for the radiative recombination from two main emission types where the energy state of F^+ center (*i.e.* one electron trapped at an oxygen vacancy) and carbonyl radical causing UV and blue light are located within the wide band gap of aluminum hydroxide.[4,12,14,16–18,29–33] Additional PLE spectra of Sample-A and B monitored at 390 nm wavelength are in Fig. S1(a) and (b).† In amorphous aluminum hydroxide materials, F^+ center emits the PLE peak at 370 nm.[12,14,16–18] Due to the oxygen defect, the material loses its crystallinity and become amorphous. Fig. 2 shows the

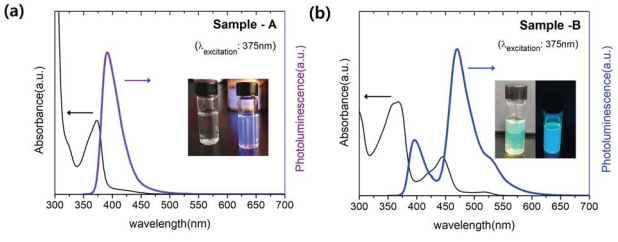

Fig. 1 Absorption and PL spectra of (a) Sample-A and (b) Sample-B dispersed in hexane at room temperature. Emitted solutions under ambient light (left side) and a 365 nm UV lamp (right side) were shown in images for each graph.

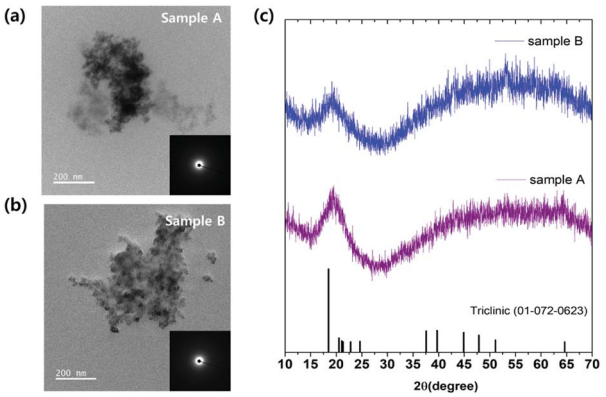

Fig. 2 FE-TEM images of Sample-A (a) and B (b) nanoparticles. (c) XRD patterns of $Al(OH)_3$ (ICDD: 01-072-0623), Sample-A and B in order from the bottom up.

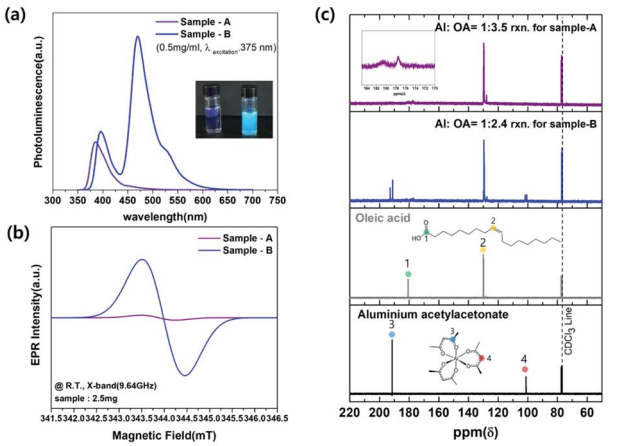

Fig. 3 (a) PL spectra of Sample-A and B at the same concentrations (0.5 mg mL^{-1}) dispersed in hexane. The inset images of samples emitted under 365 nm UV light at room temperature. (b) X-band (9.64 GHz) EPR spectra of Sample-A (violet color) and -B (blue color) powder at room temperature. (c) ^{13}C NMR spectra of initiators before synthesis of Sample-A or B, oleic acid, and aluminum acetylacetonate (from the top spectrum down).

morphology properties of two amorphous $Al(OH)_{3-x}$ nanoparticles we fabricated. Field emission-transmission electron microscopy (FE-TEM) images provided further details of cross-linked nanoparticles with a size of ≈9.0 nm in diameter for two samples. Selected area electron diffraction (SAED) patterns presented as insets of FE-TEM images in Fig. 2(a) and (b) point out the predominantly amorphous phase of two samples. The synthesized amorphous Sample-A and B nanoparticles were also confirmed the amorphous phase supported by the broadened peaks in their XRD patterns as shown in Fig. 2(c), which generally matches the bulk triclinic crystal system (ICDD: 01-072-0623). The Fourier transform infrared (FT-IR) spectrum of precursor materials ($Al(acac)_3$, oleic acid) and product samples (Sample-A and B) are shown in Fig. S1(c)† to compare the vibration absorption difference. In the two FT-IR spectra (violet and blue color) below in Fig. S1(c)† corresponding to Sample-A and B materials, Al–O and Al–OH stretching modes are shown in the 500–850 cm^{-1} and 1072–1076 cm^{-1} regions, respectively.[3] In addition, the hydroxyl stretch vibration from Al–OH is located at 3400 cm^{-1}.[16,17] Two vibration peaks located at around 1463 cm^{-1} and 1579 cm^{-1} are ascribed to the carboxylate group's asymmetric and symmetric stretching vibrations (COO^-), respectively.[12] Lower intensity around 2430 cm^{-1} was observed for two synthesized samples, which belongs to the stretching vibration of CO_2 from the decomposition of organic precursors.[6,17] And peaks located at 2850 cm^{-1}, 2920 cm^{-1}, and 3005 cm^{-1} clearly indicate the existing $-CH_2$ symmetry stretching, $-CH_2$ asymmetry stretching, and =C–H stretching, respectively.[16–18] This suggests that the oleate group from oleic acid is attached to the surface of $Al(OH)_{3-x}$ nanoparticles, which increases stability due to the long carbon chain surfactant and leads to weakly green light emission. Hydroxyl group and carbon compounds like Al–OH, CO_2, and carboxylate from the synthetic reaction on the surface of aluminum oxide/hydroxide nanoparticles can be raised green light emission.[12,16,18] The two synthesized samples exhibit the following differences in luminescence property as shown in Fig. 3(a) at the same concentrations of 0.5 mg mL^{-1} dispersed in hexane. In particular, Sample-B has higher intensity at an emissive wavelength of 465 nm than that with Sample-A. The electron paramagnetic resonance spectroscopy (EPR) was analyzed to address the presence of paramagnetic species in materials as the source of the highly luminescent PL peak of 465 nm. As shown in Fig. 3(b), 2.5 mg of Sample-A and B are measured at room temperature by EPR spectroscopy (in *x*-band at magnetic field modulation of 9.64 GHz), where the signals are shown at a magnetic field of 343.8 mT and 343.9 mT, respectively. The two magnetic field values were converted to 2.001 and 2.002 of *g* factor using resonance equation, $g = h\nu/\beta H$ (corresponding to *h*: Planck constant, β: bohr magneton, ν: frequency, and *H*: magnetic resonance field). The *g* factor value between 1.999 and 2.01 has been reported as the carbonyl radicals caused by the decomposition of metal–organic precursors in metal-hydroxide/oxide materials where the form of (–M–O–C$^\bullet$) bond exists in the lattice or surface led to luminescence between 440 and 470 nm.[6,13,16,20,21,31–33] By increasing the number of washing Sample-B nanoparticles, we confirmed that carbonyl radicals were almost on the surface of nanoparticles. After washing 20 times with methanol, it was confirmed in Fig. S2(a) and (b)† that the PLQY decreased to 37% from 67% at 465 nm, and the EPR signal intensity at 2.003 (*g* factor) intensity also decreased. In particular, the larger magnetic signal at Sample-B than Sample-A suggests a relatively large amount of carbonyl radical on the surface of Sample-B, which results in higher luminescence intensity of 465 nm as in the spectrum in Fig. 3(a). The amount of carbonyl radicals has been known to be caused by the decomposition of the aluminum acetylacetonate precursors.[17,21,31,33] ^{13}C NMR spectra are analyzed as shown in Fig. 3(c) to check the initiator affecting the carbon-related radical generation before $Al(OH)_{3-x}$ synthesis. The initiator solution mixed with $Al(acac)_3$ and oleic acid at a molar ratio of 1 : 3.5 or 1 : 2.4 used to make Sample-A or B, respectively, was produced by heating to 120 °C and degassing for 20 minutes. When

$Al(acac)_3$ and oleic acid react at a molar ratio of 1 : 3.5, Al–oleates are formed in most cases with a few aluminum acetylacetonates as confirmed by the peak positions around 180 ppm and 130 ppm for the first ^{13}C NMR spectrum (violet color) in Fig. 3(c). These are similar to No. 1 and 2 peaks located in the third spectrum of the oleic acid (Sigma Aldrich). The peak at 130 ppm corresponds to the carbon double bond, while the peak near 180 ppm corresponds to the carbon of the carboxylic acid group. The carbon position of the carboxylate group in the first ^{13}C NMR spectrum (violet color) was shifted slightly as the aluminum was connected instead of hydrogen. On the other hand, when the mixture of $Al(acac)_3$ and oleic acid were reacted at a molar ratio of 1 : 2.4 according to the above mentioned method, peaks at 190 ppm and 100 ppm of the ^{13}C NMR spectrum (second graph, blue line) in Fig. 3(a) exhibit the remaining $Al(acac)_3$, which has similar locations as the No. 3 and 4 in the ^{13}C NMR spectrum of $Al(acac)_3$ (Sigma Aldrich, 99%) according to the fourth data of Fig. 3(a). Peaks at approximately 190 ppm and 100 ppm are the carbon values close to the acetylacetonate's oxygen and the carbon between carbons connected to oxygen as shown in the fourth ^{13}C NMR spectrum image, respectively. Therefore, the remaining $Al(acac)_3$ from the mixture before Sample-B synthesis was easily decomposed at the reaction temperature of 200 °C to form the carbonyl radical, which causes higher blue light-emitting intensity of 465 nm than for Sample-A.

Application on electrically driven light-emitting devices

Aluminum oxide/hydroxide with defects has been generally applied to passive UV-pumped LEDs that produce excitation wavelength mismatch due to UV-LED chips emitting at 370–407 nm wavelengths as excitation sources.[4,13,16,17] In this work, unlike the previously reported applications, the electroluminescence of $Al(OH)_{3-x}$ we made were confirmed by direct electron injecting LEDs.[15–17] Synthesized luminescent aluminum hydroxide nanoparticles as emissive layers were first applied to electrically driven active-LEDs without using a UV chip. A schematic structure of $Al(OH)_{3-x}$ based LED devices is shown in Fig. 4(a). An organic–inorganic hybrid device architecture of [ITO (cathode)/ZnO nanoparticle films (40 nm)/$Al(OH)_{3-x}$ active layers (2 monolayers)/2,2′-bis(4-(carbazol-9-yl)phenyl)-biphenyl (BCBP, 50 nm)/MoO_3 (10 nm)/Al (100 nm, anode)] was efficiently constructed using the solution processing method. In addition, the band-energy diagram is shown in Fig. 4(b), the location of the conduction-band minimum (CBM) and valence-band maximum (VBM) were retrieved from ultraviolet photoelectron spectroscopy (UPS) and UV-vis absorption spectroscopy. In the case of $Al(OH)_{3-x}$ we made as the emissive layer, a VBM of −7.35 eV was obtained from UPS data in Fig. S3(a)† using the relationship VBM = 21.22 eV − (E_{cutoff} − E_{onset}), where 21.22 eV ($h\nu$) corresponds to the incident energy from the He I radiation source, E_{cutoff} to the high binding energy shown on the right side of the spectrum, and E_{onset} to VB-region energy onset shown on the left side of the spectrum. We also used the Tauc plot from UV-vis absorption spectrum of $Al(OH)_{3-x}$ to determine the position of CBM at −3.36 eV below the vacuum level using the relationship of CBM = E_g − VBM, where E_g corresponds to an optical band gap clarified from the excitation peak of the Tauc plot shown in Fig. S3(b).† The electron–hole recombination trap states are also located at −5.00 eV, −4.70 eV, and −4.10 eV below the vacuum level. ZnO nanoparticles with 2.7 nm in diameter, as shown in Fig. S4(a),† were used as ETL to facilitate transport electrons to the $Al(OH)_{3-x}$ emissive layer with a large bandgap. Furthermore, the smaller the size of ZnO, the higher the CBM, which makes it easier to inject electrons into the emissive layer owing to the quantum confinement effect of ZnO.[8,24] Fig. S4(b) and (c)† show the UPS spectrum and Tauc plot of the synthesized ZnO nanoparticles. We confirmed that the position of the VBM and CBM is −7.87 eV and −3.97 eV below the vacuum level, respectively using relationships as mentioned above VBM = 21.22 eV − (E_{cutoff} − E_{onset}) and CBM = E_g − VBM. BCBP with a deep HOMO level of −6.2 eV was selected in consideration of the deep VBM position of $Al(OH)_{3-x}$ for easy hole transport and was expected to be possible for electron blocking due to the higher LUMO level of −2.6 eV. The optoelectrical properties of devices with Sample-A and B as emitting layers are shown in Fig. 5. Fig. 5(a)

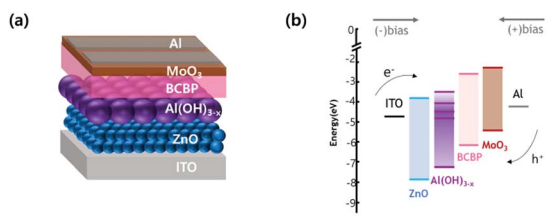

Fig. 4 Schematic illustrations of (a) device architecture and (b) energy band diagram of $Al(OH)_{3-x}$ based LED with inverted device structure of [ITO/ZnO nanoparticle films (40 nm)/emissive active layers/BCBP (50 nm)/MoO_3 (10 nm)/Al (100 nm)]. ZnO and emissive $Al(OH)_{3-x}$ layers were prepared by spin-casting and BCBP, MoO_3, and Al were thermally evaporated on top of the spun-cast ZnO/$Al(OH)_{3-x}$ layers.

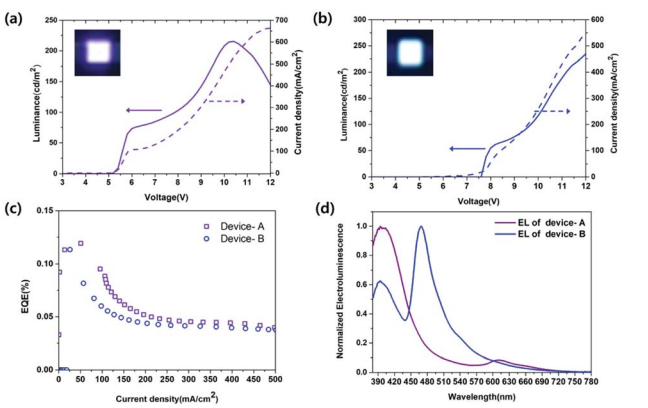

Fig. 5 Characteristics of devices applied with Sample-A and B EML: (a) J–V–L curves of device with Sample-A EML and the emissive pixel of Device-A. (b) J–V–L characteristics for the Sample-B based device and the inset pixel image of Device-B. (c) The EQE (%) *vs.* current density behavior of Device-A (opened square, violet color) and Device-B (opened circle, blue color). (d) EL spectrum of Device-A (violet) and -B (blue).

shows the Device-A performance of the current density–voltage–luminance (J–V–L), and the pixel image of the device are depicted. The device reached the turn-on voltage of 5.6 V and the maximum luminance of 215.48 cd m^{-2}. The maximum EQE of 0.12% at 50.54 mA cm^{-2} are shown in Fig. 5(c). The electroluminescence spectrum of Device-A, mainly emitting 390 nm UV-light driven at 5.6 V is presented in Fig. 5(d). Additionally, the peak appears around 590–780 nm (2.1–1.6 eV) in EL spectra due to exciplex emission (*i.e.*, interfacial recombination between organic and inorganic layer due to high injection barrier) that is originated from the recombination transition at the interface between trap states in the emissive layer and BCBP of HTL.[34–37] The J–V–L graph and the luminance pixel photo of the device with Sample-B emissive layer shown in Fig. 5(b) exhibit the turn-on voltage as around 8.2 V and have luminance up to 133.49 cd m^{-2}. In addition, it is confirmed in Fig. 5(c) that the EQE of 0.09% reached the maximum at a current density of 33.12 mA cm^{-2}. The electroluminescence spectrum of Device-B, which has 465 nm of major emitting light driven at 10.4 V is presented in Fig. 5(d).

Electrically driven LEDs with $Al(OH)_{3-x}$ nanoparticles as emissive layer we presented without incurring the burden of intrinsic toxicity or elemental scarcity can be expected to replace rare-earth luminophores and contribute to the development of display technology due to their chemical stability, optical properties, and EL properties.

Experimental

Materials and synthetic methods

Materials. Aluminum acetylacetonate (Sigma Aldrich, 99%), 1-octadecene (Sigma Aldrich, 90%), oleic acid (Sigma Aldrich, 90%), lithium bis(trimethylsilyl)amide solution 1.0 M in hexanes (Sigma Aldrich), dimethylsulfoxide (Sigma Aldrich, 99.9%), zinc acetate dihydrate (Sigma Aldrich, 98%), hexylamine (Sigma Aldrich, 99%), ethanolamine (Sigma Aldrich, 99%) ethanol (Sigma Aldrich, 99.5%) tetramethyl ammonium hydroxide pentahydrate (Sigma Aldrich, 97%), 2,2′-bis(4-(carbazol-9-yl)phenyl)-biphenyl (BCBP, OSM 99.9%), MoO_3 (Taewon Scientific, 99.95%), Al (Taewon Scientific, 99.999%).

Synthesis of $Al(OH)_{3-x}$ nanoparticles (Sample-A). 0.5 mmol of $Al(acac)_3$, 1.75 mmol (1.2 mmol for Sample-B) of oleic acid, and 10 mL of 1-octadecene were placed in a 100 mL round flask and heated to 120 °C, and degassed for 20 minutes. At an elevated temperature of 200 °C, 0.25 mL (0.4 mL for Sample-B) of lithium bis(trimethylsilyl)amide solution were injected into the mixture reaction flask under N_2 ambient. After 10 minutes, the flask was cooled to room temperature to stop the reaction. The product solution was washed using methanol, and the purification process was repeated several times with 10 000 rpm speed and 4 min duration in each purification. After centrifugation, the supernatant was removed to collect nanoparticle sticky powder. The collected nanoparticles were finally redispersed in hexane.

Synthesis of ZnO nanoparticles with a diameter of 2.7 nm. 4 mmol of $Zn(OAc)_2 \cdot 2H_2O$, 0.07 mL of hexylamine and 0.24 mL of ethanolamine were dissolved in 10 mL of DMSO and heated to 80 °C in air condition with strongly stirring. 5 mmol of TMAH dissolved in 10 mL of ethanol was rapidly injected into the zinc acetate solution at 80 °C. Then, the reactor was cooled immediately after injection to stop the growth. The reaction mixture was washed with acetone several times and purified ZnO nanoparticles were redispersed in butanol.

Characterization

Optical properties. UV-Vis absorbance, PL, and PLE spectra of $Al(OH)_{3-x}$ samples dispersed in hexane were measured at room temperature using Agilent Cary 5000 UV-vis-NIR and ACTON spectra Pro 2150i spectrometer. The relative photoluminescence quantum yields (PLQYs) of $Al(OH)_{3-x}$ samples were estimated by comparing their fluorescence intensities with those of primary standard dye solutions with the same emission wavelength as the $Al(OH)_{3-x}$ emissive materials at the same density and excitation wavelength. Dye solutions are 9,10-diphenylanthracene ($\lambda_{max}^{PL} = 406$ nm with QY = 90% in ethanol), coumarin 6 ($\lambda_{max}^{PL} = 501$ nm with QY = 80% in ethanol), coumarin 515 ($\lambda_{max}^{PL} = 478$ nm with QY = 80% in ethanol), and rhodamine 590 ($\lambda_{max}^{PL} = 550$ nm, QY = 95% in ethanol).

Field emission transmission electron microscope. FE-TEM images of $Al(OH)_{3-x}$ and ZnO nanoparticles were viewed with JEM-F200 (JEOL) at an acceleration voltage of 200 kV to analyze their average size.

X-ray powder diffraction. The XRD patterns of purified $Al(OH)_{3-x}$ nanoparticles were collected on a new D8 advanced (Bruker) diffractometer using the Cu Kα radiation (1.54 Å) source.

Fourier transform infrared. FT-IR spectra were measured with TENSOR27 (Bruker) infrared spectrophotometer at the range of 4000–400 cm^{-1} with the powder or solution technique.

^{13}C nuclear magnetic resonance. 500 MHz ^{13}C NMR results were recorded using a Varian/Oxford As-500 spectrometer with a 5 mm IDPFG probe. All samples were dispersed in $CDCl_3$ as the solvent and measured by 1000 of scans for ^{13}C NMR analysis. He main paragraph text follows directly on here.

Electron paramagnetic resonance. The EPR measurements were done at room temperature with an EMX Plus (Bruker) spectrophotometer in the *x*-band at a magnetic field modulation of 9.64 GHz. For EPR measurements, 2.5 mg of purified Sample-A and B nanoparticles were prepared.

Ultraviolet photoelectron spectroscopy. UPS spectra of ZnO and $Al(OH)_{3-x}$ films (Fig. S3 and S4†) were collected by the AXIS SUPRA (Kratos, UK) instrument with He I radiation source (21.22 eV).

Device fabrication and characterization

Patterned ITO glass substrates were cleaned in an ultrasonic bath with acetone, deionized water, and isopropyl alcohol for 10 min each. On the cleaned substrates, ZnO nanoparticle solution in butanol (40 mg mL^{-1}) was spin-coated at 2000 rpm for 30 s and annealed at 90 °C for 30 min in oven filled with N_2 gas to form a 40 nm layer. Then, 2–3 mg mL^{-1} of Sample-A or B dispersion was spin-coated at 4000 rpm for 30 s under N_2 gas. The thickness of the $Al(OH)_{3-x}$ layer was ≈20 nm. Then, BCBP

(50 nm), MoO_3 (10 nm), and Al (100 nm) were sequentially deposited by thermal evaporation under a vacuum pressure of $<1 \times 10^{-6}$ torr with deposition rates of 0.6–1 Å s^{-1} for BCBP, 0.2 Å s^{-1} for MoO_3, and 3–6 Å s^{-1} for the Al electrode. The current–voltage–luminance (J–V–L) characteristics and the EL spectra of devices were measured with Keithley 236 source measure unit and a Konica-Minolta CS-2000 Spectroradiometer.

Conclusions

Aluminum hydroxide nanocrystals with oxygen defects and carbonyl radical impurities were synthesized by a simple method. By controlling the ratio of precursors, we obtained nanosized amorphous $Al(OH)_{3-x}$ emitting at 390 nm or mainly emitting at 465 nm with a narrow FWHM (35–43 nm) and a PLQY up to 70%. The PL peak at 390 nm was attributed to the F^+ center of amorphous aluminum hydroxide, and the emission peak of 465 nm arose from paramagnetic defects associated with carbonyl radical ($g = 2.001$–2.003). The UV–blue emissive nanoparticles we made were first applied as an emissive layer to an electrically driven active device. The electroluminescent LED device in which Sample-A was applied as an emissive layer had a brightness of up to 215.48 cd m^{-2} and an EQE of 0.12%. When Sample-B was substituted, it had a luminance of up to 133.49 cd m^{-2} and an EQE of up to 0.09%. The aluminum hydroxide ($Al(OH)_{3-x}$) we prepared is desirable to be applied in various fields such as display backlights, white-LED, bio-imaging, light therapy, counterfeit detection, and purification in the future due to their non-toxicity, low cost, chemical stability, and electroluminescent properties.

Conflicts of interest

There are no conflicts to declare.

Acknowledgements

This work was supported by Industrial Core Technology Development Program (No. 10077471) funded by the Ministry of trade, Industry & Energy (MOTIE, Korea). We also acknowledge support from Samsung Research Funding and Incubation Center of Samsung Electronics under project no. IO201214-08134-01.

References

1 W. L. Xu, M. J. Zheng, S. Wu and W. Z. Shen, *Appl. Phys. Lett.*, 2004, **85**, 4364.
2 S. Liu, L. Zhang, Y. Fan, J. Luo, P. Zhang and L. An, *Appl. Phys. Lett.*, 2006, **89**, 015911.
3 J. Gangwar, B. K. Gupta, P. Kumar, S. K. Tripathi and A. K. Srivastava, *Dalton Trans.*, 2014, **43**, 17034–17043.
4 X. Bai, G. Caputo, Z. Hao, V. T. Freitas, J. Zhang, R. L. Longo, O. L. Malta, R. A. Ferreira and N. Pinna, *Nat. Commun.*, 2014, **5**, 5702.
5 B. D. Evans and M. Stapelbroek, *Phys. Rev. B: Condens. Matter Mater. Phys.*, 1978, **18**, 7089–7098.
6 Y. Wakui, K. Takahashi, Y. J. Shan, K. Tezuka, H. Imoto, S. Hosokawa, N. Shinozaki, M. Ando and H. Maekawa, *J. Lumin.*, 2015, **157**, 137–142.
7 J. H. Kim, D. Y. Jo, K. H. Lee, E. P. Jang, C. Y. Han, J. H. Jo and H. Yang, *Adv. Mater.*, 2016, **28**, 5093–5098.
8 J. Pan, J. Chen, Q. Huang, Q. Khan, X. Liu, Z. Tao, Z. Zhang, W. Lei and A. Nathan, *ACS Photonics*, 2016, **3**, 215–222.
9 J. Gangwar, B. K. Gupta, S. K. Tripathi and A. K. Srivastava, *Nanoscale*, 2015, **7**, 13313–13344.
10 A. Hong, J. Kim and J. Kwak, *Adv. Opt. Mater.*, 2020, **8**, 2001051.
11 P. He, Y. Shi, T. Meng, T. Yuan, Y. Li, X. Li, Y. Zhang, L. Fan and S. Yang, *Nanoscale*, 2020, **12**, 4826–4832.
12 M. Kim, D. Lee, H. Y. Woo, T. H. Kim, T. Paik and K. S. Kim, *Mater. Des.*, 2019, **175**, 107800.
13 M. Y. Cuikun Lin, Z. Cheng, C. Zhang, Q. Meng and J. Lin, *Inorg. Chem.*, 2008, **47**, 49–55.
14 T. H. Li, L. Z. Liu, X. L. Wu, J. C. Shen, F. Gao and P. K. Chu, *Appl. Phys. Lett.*, 2010, **97**, 121901.
15 X. Wu, S. Xiong, J. Guo, L. Wang, C. Hua, Y. Hou and P. K. Chu, *J. Phys. Chem. C*, 2012, **116**, 2356–2362.
16 B. Chen, A. S. Susha, C. J. Reckmeier, S. V. Kershaw, Y. Wang, B. Zou, H. Zhong and A. L. Rogach, *Adv. Mater.*, 2017, **29**, 1604284.
17 B. Chen, X. Xu, S. Zou, Y. Wang, B. Zou, H. Zhong and A. L. Rogach, *Adv. Opt. Mater.*, 2017, **6**, 1701115.
18 J. Y. Chae, H. Y. Woo, M. Kim, D. Lee, D. W. Lee, K. S. Kim and T. Paik, *Dyes Pigm.*, 2020, **176**, 108201.
19 Y. Du, W. L. Cai, C. M. Mo, J. Chen, L. D. Zhang and X. G. Zhu, *Appl. Phys. Lett.*, 1999, **74**, 2951–2953.
20 T. Hayakawa, A. Hiramitsu and M. Nogami, *Appl. Phys. Lett.*, 2003, **82**, 2975–2977.
21 H. Zheng, B. Chen, L. Shi, F. Zhang, Z. Zhao, Y. Liu, L. Huang, B. Zou and Y. Wang, *Nanophotonics*, 2020, **9**, 1509–1518.
22 W. K. Bae, J. Lim, D. Lee, M. Park, H. Lee, J. Kwak, K. Char, C. Lee and S. Lee, *Adv. Mater.*, 2014, **26**, 6387–6393.
23 J. Kwak, J. Lim, M. Park, S. Lee, K. Char and C. Lee, *Nano Lett.*, 2015, **15**, 3793–3799.
24 E. Moyen, J. H. Kim, J. Kim and J. Jang, *ACS Appl. Nano Mater.*, 2020, **3**, 5203–5211.
25 F. Wang, Y. H. Chen, C. Y. Liu and D. G. Ma, *Chem. Commun.*, 2011, **47**, 3502–3504.
26 D. I. Son, B. W. Kwon, D. H. Park, W. S. Seo, Y. Yi, B. Angadi, C. L. Lee and W. K. Choi, *Nat. Nanotechnol.*, 2012, **7**, 465–471.
27 W. Kwon, Y. H. Kim, C. L. Lee, M. Lee, H. C. Choi, T. W. Lee and S. W. Rhee, *Nano Lett.*, 2014, **14**, 1306–1311.
28 Z. Luo, G. Qi, K. Chen, M. Zou, L. Yuwen, X. Zhang, W. Huang and L. Wang, *Adv. Funct. Mater.*, 2016, **26**, 2739–2744.
29 Z. Q. Yu, C. X. Wang, X. T. Gu and C. Li, *J. Lumin.*, 2004, **106**, 153–157.
30 Y. Ohta, T. Hayakawa, T. Inomata, T. Ozawa and H. Masuda, *Chem. Lett.*, 2017, **46**, 32–34.
31 Y. S. Choi, S. E. Kim, M. R. Ha, J. C. Kim, H. j. Paik, S. H. Lee and Y. I. Park, *Prog. Org. Coat.*, 2021, **151**, 105926.

32 J. Kim, D. J. Darley, W. Buckel and A. J. Pierik, *Nature*, 2008, **13**, 239–243.
33 R. A. Lalancette, D. Syzdek, J. Grebowicz, E. Arslan and I. Bernal, *J. Therm. Anal. Calorim.*, 2018, **135**, 3463–3470.
34 H. Lee, J. Kwak, C. M. Kang, Y. Y. Lyu, K. Char and C. Lee, *Opt. Express*, 2015, **23**, 11424–11435.
35 X. Yang, Y. Divayana, D. Zhao, K. S. Leck, F. Lu, S. T. Tan, A. P. Abiyasa, Y. Zhao, H. V. Demir and X. W. Sun, *Appl. Phys. Lett.*, 2012, **101**, 233110.
36 Y. Kim, C. Ippen, T. Greco, I. Jang, S. Park, M. S. Oh, C. J. Han, J. Lee, A. Wedel and J. Kim, *Electron. Mater. Lett.*, 2014, **10**, 479–483.
37 X. Huang, S. Su, Q. Su, H. Zhang, F. Wen and S. Chen, *J. Soc. Inf. Disp.*, 2018, **26**, 470–476.